

Environmental Superstatistics

G.Cigdem Yalcin^{1*} and Christian Beck²

¹*Department of Physics, Istanbul University, 34134, Vezneciler, Istanbul, Turkey*

²*School of Mathematical Sciences, Queen Mary, University of London, London E1 4NS, UK*

A thermodynamic device placed outdoors is subject to a variety of different temperatures given by short-term (daily) and long-term (seasonal) variations. In the long term a superstatistical description makes sense, with a suitable distribution function $f(\beta)$ of inverse temperature β over which ordinary statistical mechanics is averaged. We show that $f(\beta)$ is very different at different geographic locations, and typically exhibits a double-peak structure for long-term data. For some of our data sets we also find a systematic drift due to global warming.

I. INTRODUCTION

In nonequilibrium statistical mechanics, the superstatistics technique [1] is a powerful tool to describe a large variety of complex systems for which there is a change of environmental conditions and temperature fluctuations on a large scale [2–10]. A superstatistical complex system is mathematically described as a superposition of several statistics, one corresponding to local equilibrium statistical mechanics and the other one corresponding to a slowly varying parameter β of the system. Essential for this approach is the fact that there is sufficient time scale separation, i.e. the local relaxation time of the system must be much shorter than the typical time scale on which β changes. Many interesting applications of the superstatistics concept have been worked out for a variety of complex systems, for example the analysis of train delay statistics [11], hydrodynamic turbulence [12], cancer survival statistics [13] and some other applications as well, see [14–19].

In this paper we want to deal with environmental aspects of superstatistics, in the sense that we ask what distributions of inverse temperatures are seen by thermodynamic devices that are kept in open air outside a constant-temperature environment. Clearly this question is technically very relevant as many devices need to operate under strong temperature fluctuations, as given by either daily temperature fluctuations, or seasonal variations, or even long-term climatic changes. We will analyse in detail inverse temperature distributions at various geographic locations. These environmentally important distributions are different from standard examples of distribution functions discussed so far in the literature, such as the χ -square, inverse χ -square or lognormal distribution [2]. As it is well-known, superstatistics based on χ -square distributions leads to q -statistics [20, 21], whereas other distributions lead to something more complicated. A major difference is that the environmentally observed probability densities of inverse temperature typically exhibit a double-peak structure, thus requiring a different type of superstatistics than what has been done so far. In the original setting described in [1], the analysis was based on single-peaked distributions with a sharp maximum [1]. For environmentally relevant temperature distributions, this concept has to be broadened, as we shall see in the following.

II. OBSERVED INVERSE TEMPERATURE DISTRIBUTIONS—MONTHLY DATA

When looking of temperature distributions as given by real data, one clearly has to specify the relevant time scale first. Short-term temperature distributions (dominated by daily fluctuations) are very different from long-term data (dominated by seasonal variations). For very long data records, one also has to take into account non-stationary behaviour due to climate change.

We start with short-term data. Fig. 1, 2 and 3 show as an example a time series of hourly measured inverse temperatures in Ottawa during November 2011, as well as in Vancouver during May 2011 and December 2011.

One notices a dominant frequency pattern given by 1 oscillation per 24h, corresponding to the day-night temperature differences. Superimposed to this are stochastic fluctuations due to different weather conditions. What is also clearly visible in the figures are small systematic trends. In Fig. 1 (November in Ottawa) the average inverse temperature β is slightly increasing over the month of November, since the temperature slightly decreases as winter is approaching. In Fig. 2 (May in Vancouver) the average β is slightly decreasing, since summer is approaching. No clear systematic trend is visible for the December data of Fig. 3.

* corresponding author, phone +90 212 455 57 00 ext 15489, Fax +90 212 455 5855, gcyalcin@istanbul.edu.tr

A thermodynamic device that is kept outdoors for a month will basically see a Gaussian distribution of inverse temperatures. This is illustrated in Figs. 4-6, which shows the histograms of the example time series of Figs 1-3.

The effective statistical mechanics of a thermodynamic device kept outside is described by superstatistics [1] with effective Boltzmann factors $B(E)$ of the form

$$B(E) = \int_0^{\infty} f(\beta)e^{-\beta E} d\beta \quad (1)$$

where $f(\beta)$ is a single-humped probability density around the mean inverse temperature that month, in good approximation given by a Gaussian distribution, as shown in Fig. 4-6. The integration over β yields non-Boltzmannian distributions, whose details depend on $f(\beta)$. So for example the marginal distribution of velocities of an ideal gas for which β fluctuates is not Gaussian anymore, due to the integration over β in eq. (1).

Better statistics is obtained if we sample the data of a given month over many years. We sampled hourly measured inverse temperature time series, restricted to the month of November, over the period 1966-2011 for Ottawa. Fig. 7 shows this time series (restricted to November months and joined together). The corresponding histogram is well-fitted by a Gaussian (Fig. 8).

What is interesting, however, is that there is a systematic trend. Close inspection of Fig. 7 shows already to the bare eye that the average β is slightly decreasing over the years, meaning the average November temperature has slightly increased in Ottawa over the past 50 years. Clearly, this effect is related to global warming, here measured at a particular location. The same trend of a slightly decreasing average β is also visible for the May-data of Vancouver (Fig. 9), which overall are also well fitted by a Gaussian distribution (Fig. 10). Slightly more volatile behaviour is observed in December (Fig. 11), with some outbursts to large β (some very cold days) occurring relatively frequently, see Fig. 12.

Overall, the distributions for most months are in good approximation Gaussian distributions. They describe random fluctuations around the mean temperature in that month with oscillating behaviour super-imposed due to day-night temperature differences. In addition, on very long time scales there is a small systematic drift of the mean temperature to larger values, due to climate change. A thermodynamic device, to be used only in a particular month of the year, would be typically described by a superstatistics where the relevant inverse temperature distribution $f(\beta)$ is close to a Gaussian, and where the mean of that Gaussian (and possibly also the variance) has a very small time dependence over a time scale of decades.

III. OBSERVED INVERSE TEMPERATURE DISTRIBUTIONS— YEARLY DATA

We now deal with thermodynamic devices that are kept outside during the entire year, so that full seasonal variations are becoming relevant. The observed probability distributions become more complex, depending on the climatic conditions at the particular location. Examples of time series that we investigated in somewhat more detail are shown in Figs. 13-21, these are daily measured inverse mean temperatures in various locations sampled over many years. Clearly, the day-night oscillations are now less relevant, and what becomes dominating are seasonal variations [22–24]. The data now have a dominating frequency corresponding to 1 oscillation per 365 days due to seasonal variations, modulated by stochastic fluctuations due to different weather conditions on a time scale of days, plus large-scale annual fluctuations (some years warmer or colder than others) and systematic trends due to climate change.

We have investigated time series data for 8 different locations in different climatic zones. These are Darwin (Northern Territory, Australia) (1975-2011) [27], Santa Fe (1998-2011) [28], Dubai (1974-2011) [29], Sydney (1910-2011) [27], Central England (London, Bristol, Lancashire) (1910-2011) [30, 31], Vancouver (1937-2011) [32], Hong Kong (1997-2011) [33], Ottawa (1939-2011) [32], and Eureka (Nunavut, Canada) (1951-2011) [32], respectively.

These time series are heavily influenced by seasonal variations and fluctuations around the typical yearly behaviour. Interesting enough, for some locations a systematic trend (a decrease in the average inverse temperature over the years) is again visible to the bare eye. The locations where such a systematic trend is clearly seen are Dubai (Fig. 15), Sydney (Fig. 16), Vancouver (Fig. 18), Ottawa (Fig. 20), and Eureka (Fig. 21). Obviously these are local manifestations of the effects of global warming.

Figs. 22-30 show the histograms of inverse temperature time series for the various locations. These distributions are the ones relevant for the superstatistical description of thermodynamic devices that need to work in the open air and that are supposed to work properly for continuous operation over many years. The details of the distribution heavily depend on the climate zone of the location.

A typical observation is now that the relevant distributions have a double-peak structure, at least for non-tropical locations. Broadly, the left peak (small β) corresponds to summer and the right peak (large β) to winter. The entire distribution can be very roughly regarded as a superposition of two Gaussians, with some intermediate behaviour

<i>Location and time period</i>	<i>Summer(Celcius)</i>	<i>Winter(Celcius)</i>	β_1	β_2
Darwin (1975-2011)	28.32	-	1.8	-
Santa Fe (1998-2011)	22.06	3.31	18	4
Dubai (1974-2011)	33.03	20.39	7	8
Sydney (1910-2011)	20.22	13.78	2	3.5
Central England (1910-2011)	14.26	7.12	3.6	1.4
Vancouver (1937-2011)	15.80	7.05	5	2
Hong Kong (1997-2011)	27.99	19.31	10	2.7
Ottawa (1939-2011)	18.49	-1.04	12	2.1
Eureka (1951-2011)	4.21	-36.3	43	5.5

TABLE I: Maxima (in degree Celsius) and variance parameters β_1, β_2 of the two Gaussians $\sim e^{-\beta_i(\beta-\bar{\beta})^2}$ used in the fits.

between the peaks. This intermediate behaviour is more pronounced for geographical locations that have big differences between summer and winter temperatures.

Apparently, for climates with strong differences of winter and summer temperatures the two peaks of our Gaussian fits (Fig. 22-30) are far apart. Table 1 lists the two temperatures where the two maxima in the histogram occur. They are consistent with an average temperature observed during a couple of months corresponding to summer and winter, respectively, at the different geographical locations.

One may try to fit the data by other functional forms than a superposition of two Gaussians. For example, the histogram of daily measured inverse mean temperature in Dubai 1974-2011 (Fig. 31) is well fitted by an exponential $e^{-V(\beta)}$ of a double-well potential $V(x) \sim (C_2x^2 + C_3x^3 + C_4x^4)$. Generally, however, there is no simple analytic expression for the environmentally relevant inverse temperature distributions.

IV. INTERPRETATION OF RESULTS IN TERMS OF KÖPPEN CLIMATE CLASSIFICATION SYSTEM

Our superstatistical distributions are consistent with the Köppen climate classification system [34–36] which is one of the most widely used climate classification systems. In the following we will briefly review this scheme and then interpret our long-term superstatistical distributions in the Köppen context. Of course, so far our investigation only involves temperature distributions. In future work, we intend to take into account rainfall data as well [25, 26], which can also be modeled using superstatistical techniques.

There are basically 5 different climatic groups in the Köppen scheme: Group A Tropical climates, group B Arid climates, group C Temperate climates, group D Cold climates and group E Polar climates. We have chosen at least one example in each of these groups: A: Darwin, B: Santa Fe, Dubai C: Sydney, Central England, Hongkong D: Ottawa, E: Eureka.

A second and third letter give more specific information within each of the groups. In our examples, we have collected data for the following climate types:

Aw (Tropical-Savannah): Darwin,
 BSk (Arid-Steppe-Cold): Santa Fe,
 BWh (Arid-Desert-Hot): Dubai,
 Cfa (Temperate-Without dry season-Hot summer): Sydney,
 Cfb (Temperate-Without dry season-Warm summer): Central England and Vancouver,
 Cwa (Temperate-Dry winter-Hot summer): Hong Kong,
 Dfb (Cold-Without dry season-Warm summer): Ottawa,
 ET(Polar-Tundra): Eureka.

We summarize below short characterizations of these subtypes:

Aw (Tropical-Savannah) subtype is characterized by the coldest month which has a temperature of $18^\circ C$ or more. There is no rainforest and the precipitation of the driest month is less than 100 - mean annual precipitation /25.

BSk (Arid-Steppe-Cold) subtype is characterized by mean annual precipitation equal or bigger than five times and less than ten times of the precipitation threshold. The mean annual temperature is less than $18^\circ C$.

BWh (Arid-Desert-Hot) subtype is characterized by mean annual precipitation equal or less than five times of precipitation threshold. The mean annual temperature is equal or bigger than $18^\circ C$.

Cfa (Temperate-Without dry season-Hot summer) subtype is characterized by the temperature of the hottest month being equal and bigger than 22°C and the temperature of the coldest month is between 0°C and 18°C . There is no dry season for summer and winter.

Cfb (Temperate-Without dry season-warm summer) subtype is characterized as follows: The temperature of the hottest month is bigger than 10°C and the temperature of the coldest month is between 0°C and 18°C . There is no dry season for summer and winter. There is no hot summer. The number of months where the temperature is above 10°C is equal or bigger than 4.

Cwa (Temperate - Dry winter - Hot summer): The temperature of the hottest month is equal or bigger than 22°C . The temperature of the coldest month is between 0°C and 18°C . Precipitation of the driest month in winter is less than one-tenth of precipitation of the wettest month in summer.

Dfb (Cold-Without dry season-Warm summer): The temperature of the hottest month is larger than 10°C . The temperature of the coldest month is equal or less than 0°C . There is no dry season for summer and winter and there is no hot summer. The number of months where the temperature is above 10°C is equal or bigger than 4.

ET (Polar-Tundra) subtype is characterized by the temperature of the hottest month being between 0°C and 10°C .

When looking at Fig. 22-30 and Table 1, the observed inverse temperature distributions are clearly consistent with the climate classifications of the various locations. The plot for Darwin (Fig. 22) is the only one which has only a single maximum, occurring at the very high temperature 28°C , consistent with the tropical location and the non-existence of seasonal variations. Still it is interesting to see that the distribution strongly deviates from a Gaussian, there is a pronounced tail corresponding to large β .

All other plots exhibit a double-peak structure, corresponding to summer and winter. However, it is interesting that the variance of the Gaussians that we use for the fits can be very different. For example, for Santa Fe (Fig. 23) the summer-Gaussian (on the left) has a smaller variance than the winter-Gaussian (on the right), whereas for Dubai (Fig. 25) both Gaussians have about the same variance, and finally for Sidney (Fig. 26) the summer-Gaussian (on the left) has bigger variance than the winter-Gaussian (on the right). In this way one may use our plots to provide a quantitative characterization of Köppen subtypes, or even a new classification.

The plots of Fig. 26 (Central England) and Fig. 27 (Vancouver) are very similar. This is to be expected, since both locations fall into the same climate type Cfb.

The locations of the most likely temperatures (i.e. the maxima) observed in Fig. 28-30 are consistent with typical summer and winter temperatures in Hongkong, Ottawa and Eureka. Note that these temperatures are averaged over day and night.

As already mentioned, for tropical locations, such as Darwin (Fig. 22), the two peaks merge in a single peak, as expected for regions where there is hardly any difference between summer and winter temperatures. On the other hand, for polar locations, the two peaks are strongly separated, as shown in Fig. 30. for the example of Eureka. Here the two Gaussians are very far apart from each other. We suggest to use the variance of the winter- and summer-Gaussians, as well as their distance, as useful quantitative measures to characterize the temperature profile of various climate types. For example, Sydney seems special since it is the only example where the summer-Gaussian has significantly higher variance than the winter-Gaussian. Dubai seems special as well, since both winter and summer-Gaussian seem to have roughly the same variance. This allows for an alternative fit with the exponential of a double-well potential (Fig. 31).

V. SUPERSTATISTICS WITH DOUBLE-PEAKED DISTRIBUTIONS

The original concept of superstatistics provided an approximation method for sharply peaked temperature distributions, which resulted in a perturbative expansion around the Boltzmann-Gibbs limiting case [1]. Apparently, environmental superstatistics does not have sharply peaked distributions $f(\beta)$, but as we saw in the previous section there are broad distributions that often have two maxima. Hence the effective Boltzmann factors $B(E) = \int f(\beta)e^{-\beta E}d\beta$ can only be evaluated numerically. One idea would be to effectively separate the two maxima and to do a superposition of two single-peaked superstatistics, one for the summer and one for the winter. This is particularly useful if the thermodynamic device is supposed to work in one season with a particular performance, and in the other season with another one. This concept basically boils down to consider conditional temperature distributions, conditioned on the season of the year.

Another interesting question one can ask for environmental superstatistics is the large-energy asymptotics of the generalized Boltzmann factors $B(E)$. One can apply the techniques of [3] to determine, at least in principle, the decay of $B(E)$ with E for large E . For this the small- β behavior of $f(\beta)$ is relevant. For example, if $f(\beta) \sim \beta^{\gamma}$ for small β , then the generalized Boltzmann factors decay with a power law for large E , the power law exponent being related to γ [3]:

$$B(E) \sim E^{-\gamma-1} \quad (2)$$

Tsallis q -statistics [20, 21] is a particular example, with $q = \langle \beta^2 \rangle / \langle \beta \rangle^2$ [1]. In practice, for this one would need very precise data of $f(\beta)$ for small β , which in our environmental interpretation corresponds to the statistics of hot summers. The extreme-event statistics of very hot summers determines the asymptotic large- E behaviour of the effective thermostatics of the statistical mechanics device under consideration. Thus, to decide on the asymptotic behaviour of environmentally relevant $B(E)$ a systematic investigation of extreme events is needed, namely that of very hot summers.

VI. GLOBAL WARMING

As we have already mentioned before, in some of our data one sees a systematic trend which can be associated with global warming. As it is well-known, global warming is the rise in the average temperature of the Earth's atmosphere and of the oceans since the late 19th century and its projected continuation. It is primarily caused by increasing concentrations of greenhouse gases produced by human activities such as the burning of fossil fuels and deforestation. It comes with sea level rises and widespread decreases in snow and ice extent.

Quantitatively, the Earth's average surface temperature rose by 0.74 ± 0.18 °C over the period 1906-2005 [37–39]. The rate of warming over the last half of that period was almost double that of the period as a whole (0.13 ± 0.03 °C per decade, versus 0.07 ± 0.02 °C per decade). The urban heat island effect is very small and accounts for less than 0.002 °C of warming per decade since 1900 [37]. Temperatures in the lower troposphere have increased between 0.13 and 0.22 °C (0.22 and 0.4 °F) per decade since 1979, according to satellite temperature measurements [38]. Arctic regions are especially vulnerable to the effects of global warming, as has become apparent in the melting sea ice in recent years. Climate models predict much greater warming in the Arctic than the global average [39].

If sampled over many decades, the precision of some of our data is good enough to reveal the effects of global warming. As an example we show in Fig. 32 the average of daily measured mean temperature of every single year in Eureka, Nunavut, Canada from 1951-2011. This is an arctic region and our plot shows that the average temperature grows by 0.92 °C per decade (Fig. 33). So in this polar region the warming occurs at a much higher rate than the global warming rate that is averaged over the entire earth.

For some of the other locations we also observe a systematic increase in average temperature (Figs. 34-37). For Dubai (Fig. 34) the rate is also rather high, 0.63 °C per decade. For Sydney (Fig. 35), Vancouver (Fig. 36), and Ottawa (Fig. 37) one has rates comparable to the average global warming rate, namely 0.13 , 0.11 and 0.18 °C per decade, respectively. It is in the remit of the superstatistics approach that it can very well model both stochastic effects as well as systematic drifts, as long as there is a clear separation of time scales.

-
- [1] C. Beck and E.G.D. Cohen, *Physica A* **322**, 267 (2003)
 - [2] C. Beck, E.G.D. Cohen, and H.L. Swinney, *Phys. Rev. E* **72**, 056133 (2005)
 - [3] H. Touchette and C. Beck, *Phys. Rev. E* **71**, 016131 (2005)
 - [4] C. Tsallis and A.M.C. Souza, *Phys. Rev. E* **67**, 026106 (2003)
 - [5] P. Jizba, H. Kleinert, *Phys. Rev. E* **78**, 031122 (2008)
 - [6] P.-H. Chavanis, *Physica A* **359**, 177 (2006)
 - [7] S.A. Frank and D.E. Smith, *Entropy* **12**, 289 (2010)
 - [8] C. Anteneodo and S.M. Duarte Queiros, *J. Stat. Mech.* P10023 (2009)
 - [9] E. Van der Straeten and C. Beck, *Phys. Rev. E* **80**, 036108 (2009)
 - [10] R. Hanel, S. Thurner, and M. Gell-Mann, *PNAS* **108**, 6390 (2011)
 - [11] K. Briggs, C. Beck, *Physica A* **378**, 498 (2007)
 - [12] C. Beck, *Phys. Rev. Lett.* **98**, 064502 (2007)
 - [13] L. Leon Chen, C. Beck, *Physica A* **387**, 3162 (2008)
 - [14] A.Y. Abul-Magd, G. Akemann, P. Vivo, *J. Phys. A Math. Theor.* **42**, 175207 (2009)
 - [15] K.E. Daniels, C. Beck, and E. Bodenschatz, *Physica D* **193**, 208 (2004)
 - [16] C. Beck, *Physica A* **331**, 173 (2004)
 - [17] S. Rizzo and A. Rapisarda, *AIP Conf. Proc.* **742**, 176 (2004)
 - [18] D.N. Sobyenin, *Phys. Rev. E* **24**, 051128 (2011)
 - [19] P.D. Dixit, arXiv:1210.3015
 - [20] C. Tsallis, *J. Stat. Phys.* **52**, 479 (1988)
 - [21] C. Tsallis, *Introduction to Nonextensive Statistical Mechanics*, Springer (2009)
 - [22] V. Lucarini, T. Nanni, A. Speranza, *Nuovo Cimento C* **27**, 285 (2004)
 - [23] M.R. Attolini, S. Ceccinni, M. Galli, *Nuovo Cimento C* **7**, 245 (1984)
 - [24] K.Y. Vinnikov, A. Robock, N.C. Grody, A. Basist, *Geophys. Res. Lett.* **31**, L06205 (2003)

- [25] A. Porporato, G. Vico, P.A. Fay, *Geophys. Res. Lett.* **33**, L15402 (2006)
- [26] M.R. Jones, H.J. Fowler, C.G. Kilsby, S. Blenkinsop, *Int. J. Climatology* (2012), DOI: 10.1002/joc.3503
- [27] Australian Government Bureau of Meteorology www.bom.gov.au
- [28] National Oceanic and Atmospheric Administration, National Climatic Data Center www.ncdc.noaa.gov
- [29] Dubai Meteorology Office www.dia.ae
- [30] D.E. Parker, T.P. Legg, and C.K. Folland. A new daily Central England Temperature Series, 1772-1991. *Int. J. Clim.*, Vol 12, 317-342 (1992)
- [31] United Kingdom National Weather Service www.metoffice.gov.uk
- [32] Environment Canada Weather Office www.weatheroffice.gc.ca
- [33] Hong Kong Observatory, The Government of the Hong Kong Special Administrative Region www.hko.gov.hk
- [34] W. Köppen, *Meteorologische Zeitschrift*, **20**, 3, 351 (2011)
- [35] M. Kottek, J. Grieser, C. Beck, B. Rudolf, F. Rubel, *Meteorologische Zeitschrift*, **15**, 3, 259 (2006)
- [36] M. C. Peel, B. L. Finlayson, T. A. McMahon, *Hydrol. Earth Syst. Sci.*, **11**, 1633 (2007)
- [37] Trenberth et al., Ch. 3, Observations: Atmospheric Surface and Climate Change, Section 3.2.2.2: Urban Heat Islands and Land Use Effects, p. 244, in IPCC AR4 WG1 2007.
- [38] Jansen et al., Ch. 6, Palaeoclimate, Section 6.6.1.1: What Do Reconstructions Based on Palaeoclimatic Proxies Show?, pp. 466-478, in IPCC AR4 WG1 2007.
- [39] S.J. Hassol, *Impacts of a warming Arctic: Arctic Climate Impact Assessment*. Cambridge, UK: Cambridge University Press. February 2005. doi:10.2277/0521617782. ISBN 0-521-61778-2.

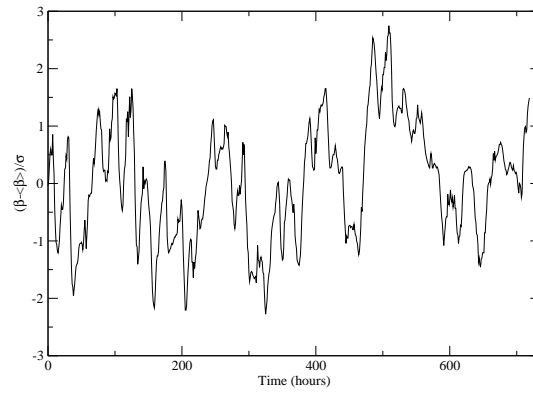


FIG. 1: Time series of hourly measured inverse temperature in Ottawa during November 2011

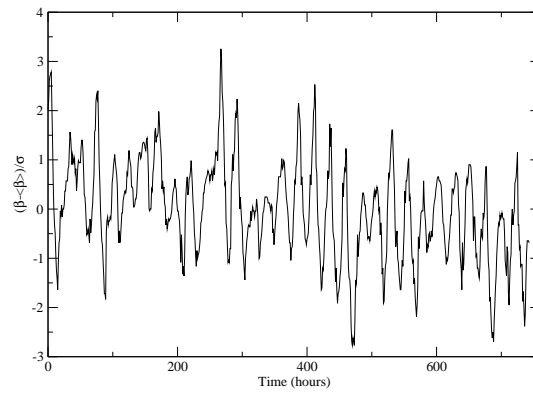


FIG. 2: Time series of hourly measured inverse temperature in Vancouver during May 2011

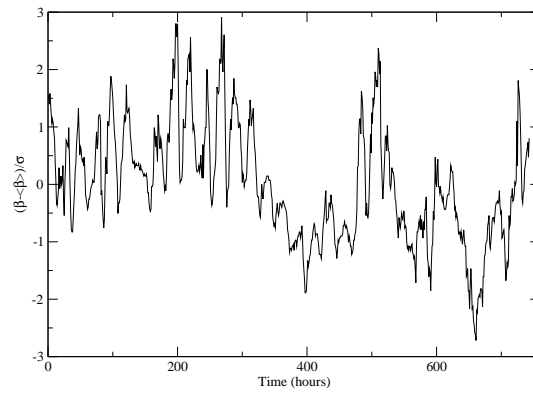


FIG. 3: Time series of hourly measured inverse temperature in Vancouver during December 2011

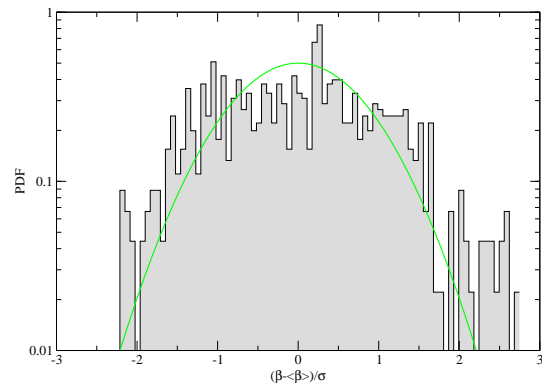


FIG. 4: Gaussian fit to the histogram of the hourly measured inverse temperature in Ottawa during November 2011

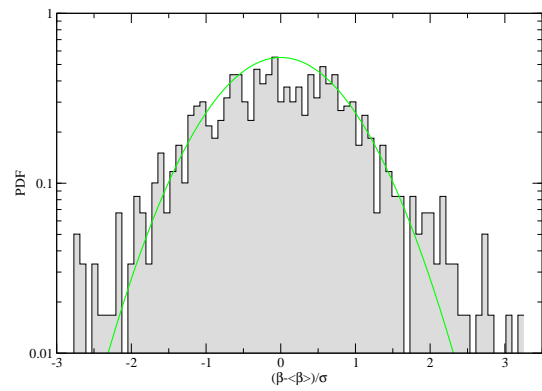


FIG. 5: Gaussian fit to the histogram of the hourly measured inverse temperature in Vancouver during May 2011

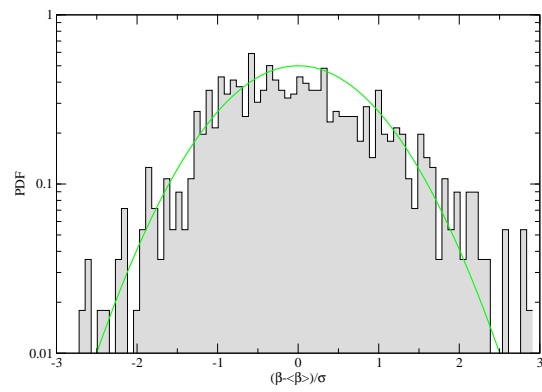


FIG. 6: Gaussian fit to the histogram of the hourly measured inverse temperature in Vancouver during December 2011

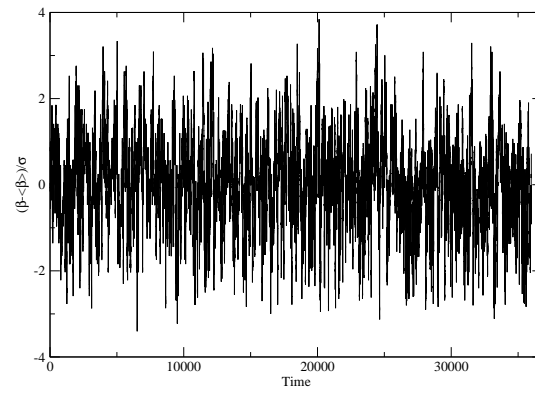


FIG. 7: Time series of hourly measured inverse temperature in Ottawa for November, sampled from 1962 to 2011 for 50 years

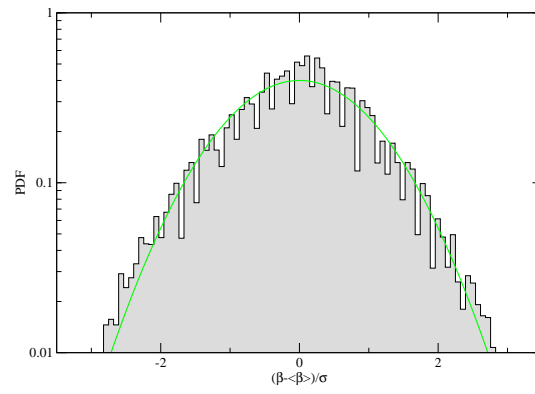


FIG. 8: Gaussian fit to the histogram of the hourly measured inverse temperature in Ottawa for 50 November months

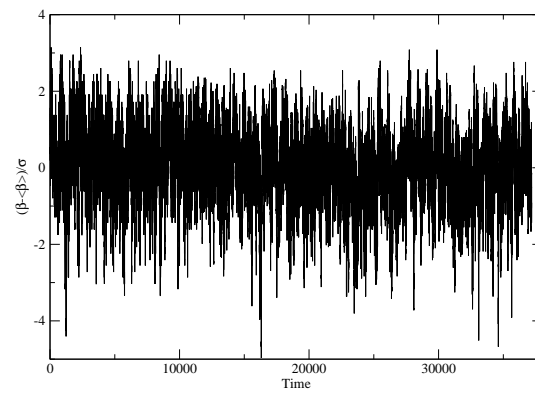


FIG. 9: Time series of hourly measured inverse temperature in Vancouver for 50 months of May

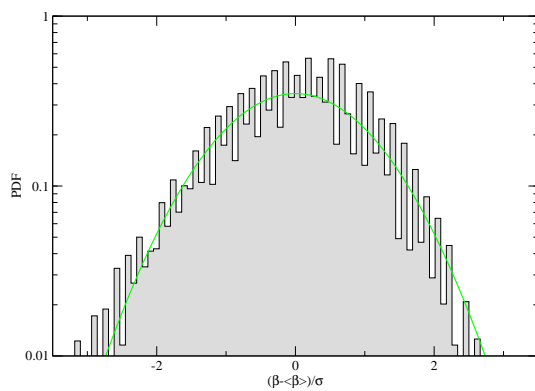


FIG. 10: Histogram the hourly measured inverse temperatures in Vancouver for 50 months of May

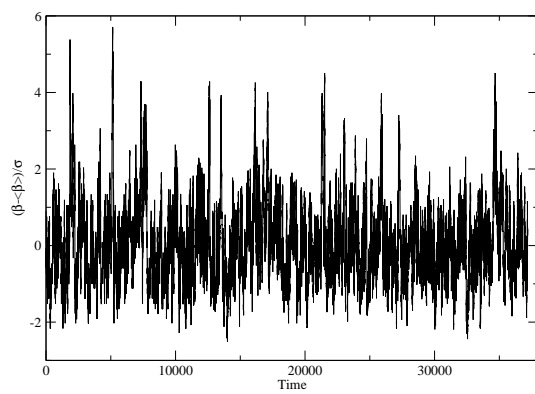


FIG. 11: Same as Fig. 9 but for December

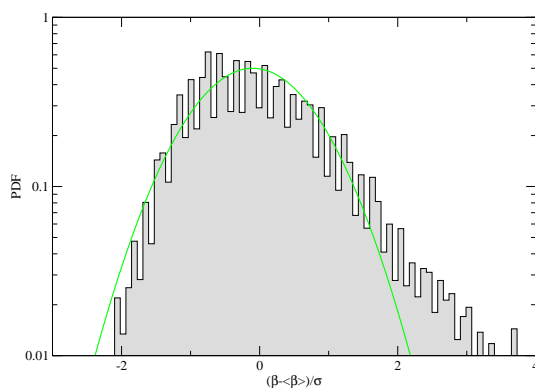


FIG. 12: Same as Fig. 10 but for December

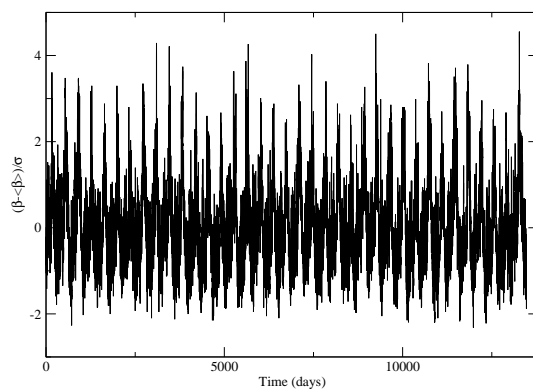


FIG. 13: Time series of daily measured inverse mean temperature in Darwin during 1975-2011

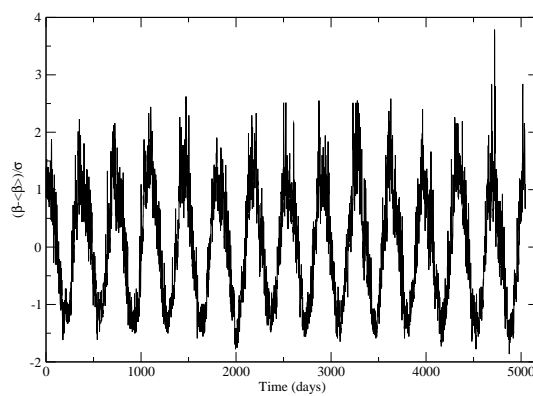


FIG. 14: Daily measured inverse mean temperature in Santa Fe 1998-2011

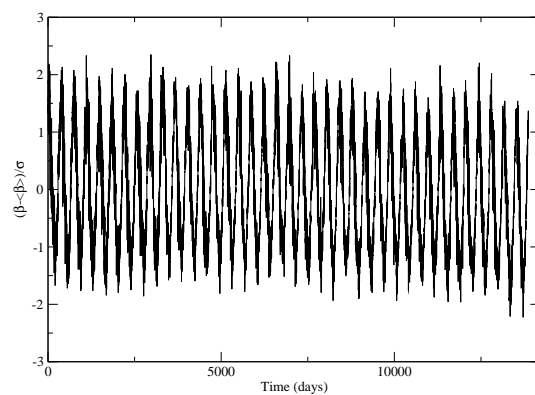


FIG. 15: Daily measured inverse mean temperature in Dubai 1974-2011

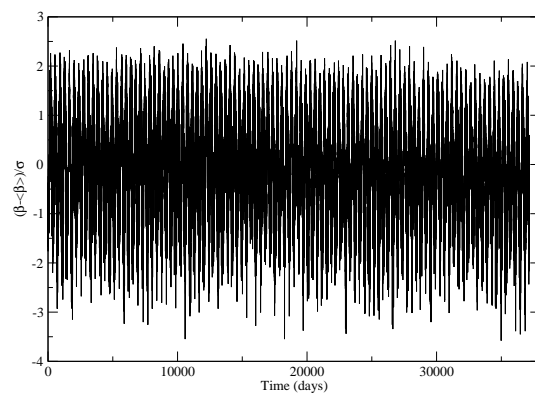


FIG. 16: Daily measured inverse mean temperature in Sydney 1910-2011

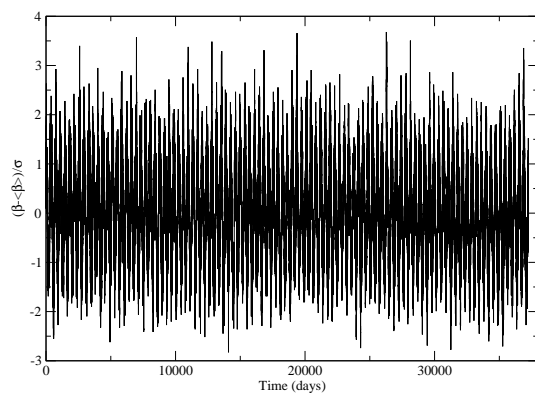


FIG. 17: Daily measured inverse mean temperature in Central England (Lancashire, London and Bristol) 1910-2011

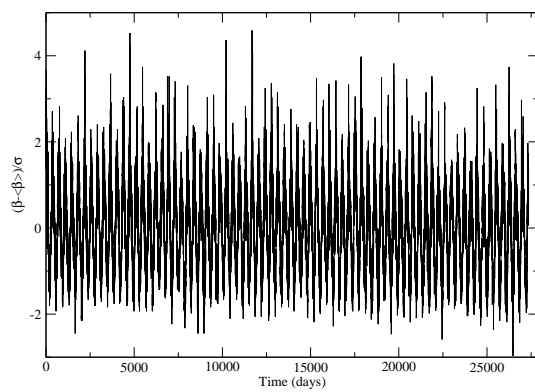


FIG. 18: Daily measured inverse mean temperature in Vancouver 1937-2011

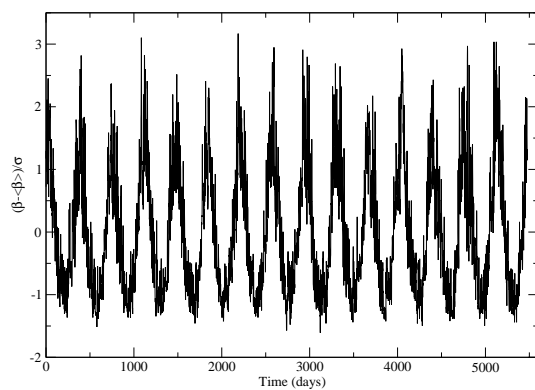


FIG. 19: Daily measured inverse mean temperature in Hong Kong 1997-2011

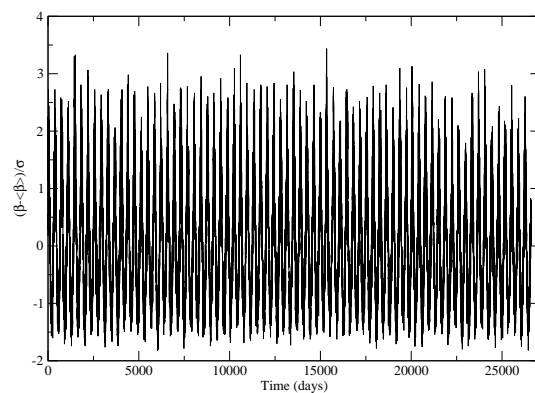


FIG. 20: Daily measured inverse mean temperature in Ottawa 1939-2011

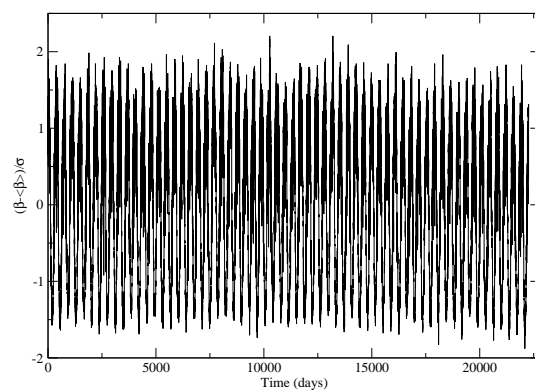


FIG. 21: Daily measured inverse mean temperature in Eureka 1951-2011

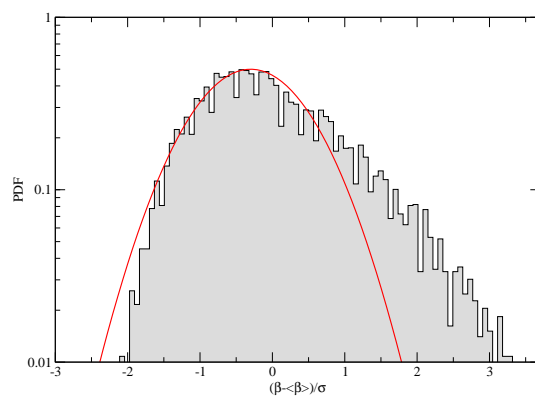


FIG. 22: Distribution of the daily measured inverse mean temperature in Darwin for 1975-2011

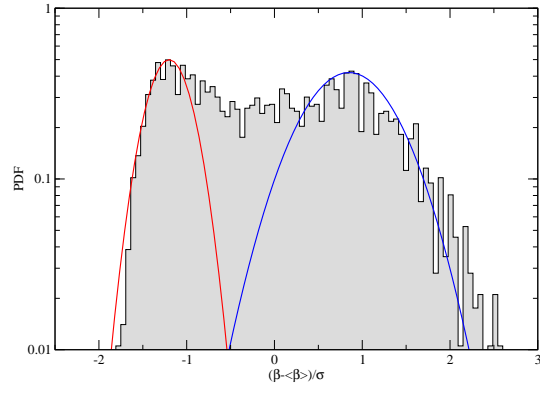


FIG. 23: Distribution of the daily measured inverse mean temperature in Santa Fe for 1998-2011

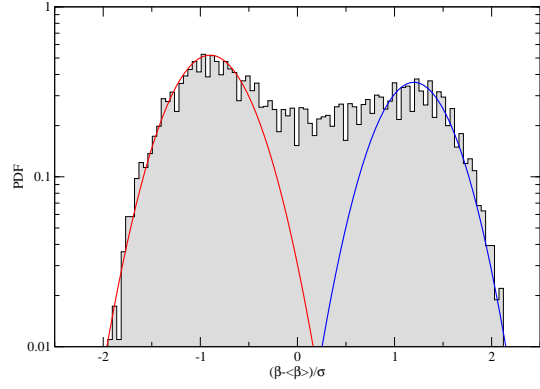


FIG. 24: Distribution of the daily measured inverse mean temperature in Dubai for 1974-2011

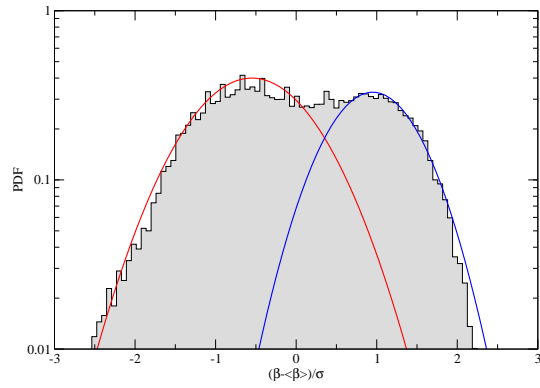


FIG. 25: Distribution of the daily measured inverse mean temperature in Sydney for 1910-2011

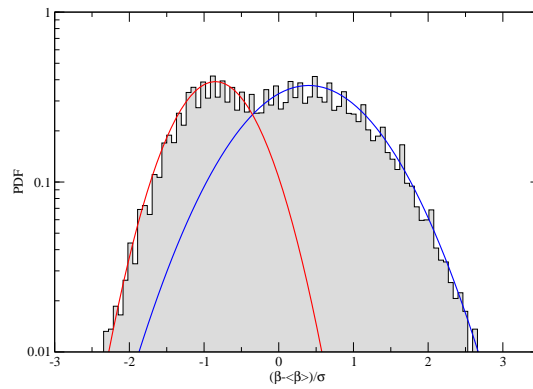


FIG. 26: Distribution of the daily measured inverse mean temperature in Central England (Lancashire, London and Bristol) for 1910-2011

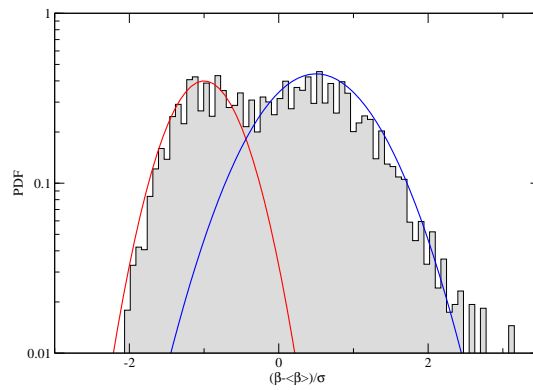


FIG. 27: Distribution of the daily measured inverse mean temperature in Vancouver for 1937-2011

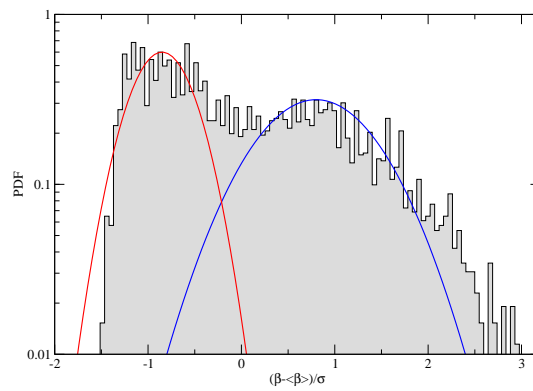


FIG. 28: Distribution of the daily measured inverse mean temperature in Hong Kong for 1997-2011

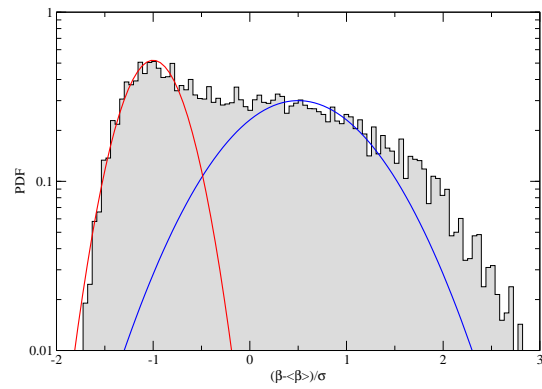


FIG. 29: Distribution of the daily measured inverse mean temperature in Ottawa for 1939-2011

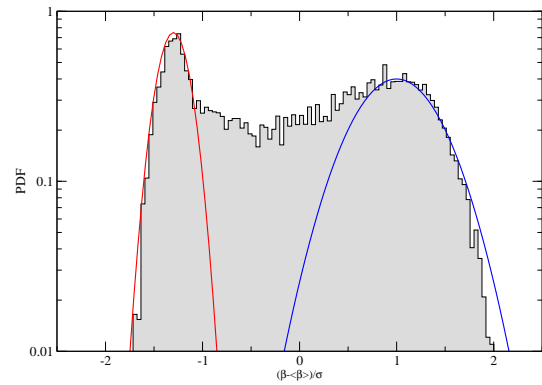


FIG. 30: Distribution of the daily measured inverse mean temperature in Eureka for 1951-2011

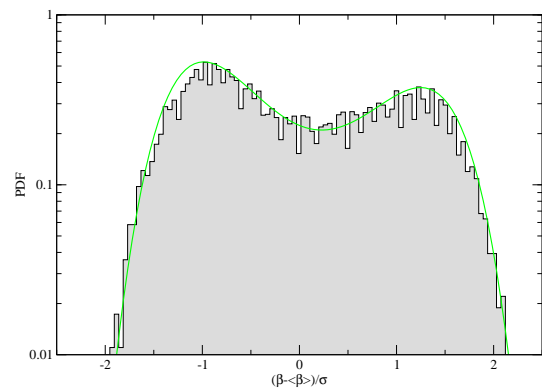


FIG. 31: Fit with the exponential of a double-well potential to the histogram of the daily measured inverse mean temperature in Dubai 1974-2011

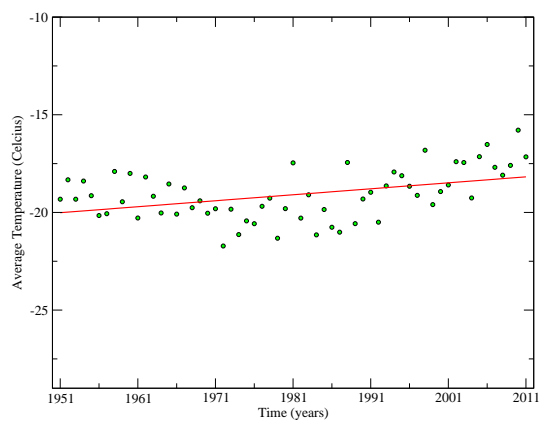


FIG. 32: Average of daily measured mean temperature of every single year in Eureka 1951-2011

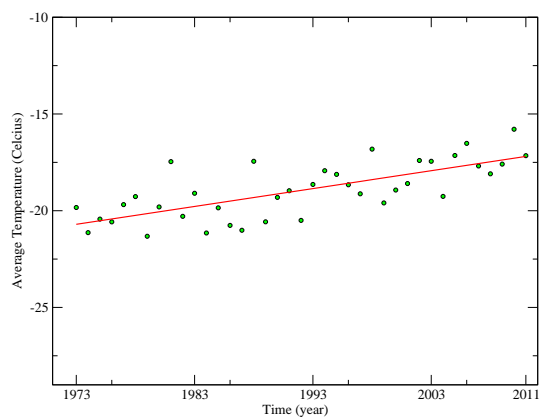


FIG. 33: Average of daily measured mean temperature of every single year in Eureka 1973-2011

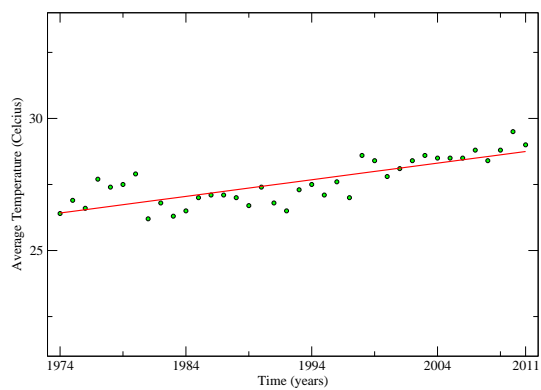


FIG. 34: Average of daily measured mean temperature of every single year in Dubai 1974-2011

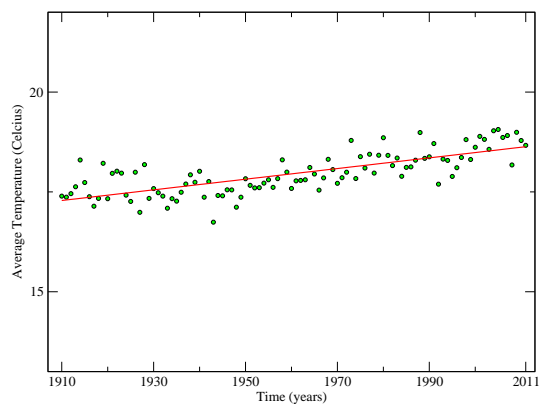


FIG. 35: Average of daily measured mean temperature of every single year in Sydney 1910-2011

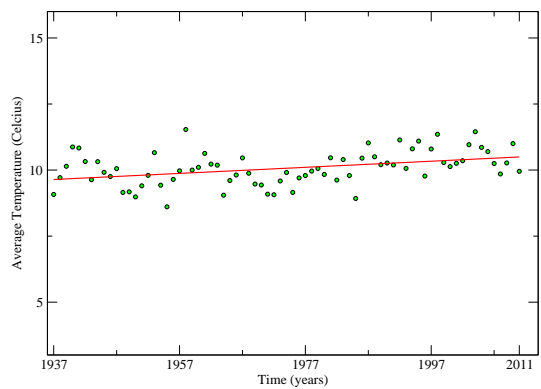


FIG. 36: Average of daily measured mean temperature of every single year in Vancouver 1937-2011

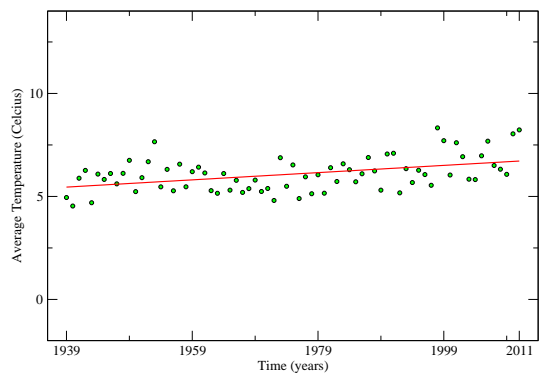


FIG. 37: Average of daily measured mean temperature of every single year in Ottawa 1939-2011